The complex-dielectric constant of sea ice at frequencies in the range 0.1–40 GHz

M. R. Vant[a)]

Environment Canada, 562 Booth Street, Ottawa, Ontario, Canada K1A OE7

R. O. Ramseier

Environment Canada, 580 Booth Street, Ottawa, Ontario, Canada K1A OH3

V. Makios

Electronics Department, Faculty of Engineering, Carleton University, Ottawa, Ontario, Canada K1S 5B6
(Received 25 October 1976; accepted for publication 29 September 1977)

A comprehensive and unique set of measurements of the complex-dielectric constant of sea ice, performed at several frequencies in the range 0.1–7.5 GHz, is described. In addition, a brief survey of previously published results is given and a set of dielectric models describing the complex-dielectric behavior of sea ice, over the frequency range 0.1–40 GHz, is discussed.

PACS numbers: 92.10.Rw, 77.20.+y, 77.40.+i

I. INTRODUCTION

Previous papers have attempted to formulate simple models[1–4] to describe the dielectric behavior of sea ice at single frequencies in the range 100 MHz to 7.5 GHz. These attempts have been hampered in part by the small quantity of published data at frequencies in this range and in part by the fact that much of what is published pertains to measurements performed on poor-quality laboratory artifacts of sea ice (see Table I).

As can be seen in Table I, this paper attempts to fill a gap in the published data for actual sea ice to extend some of the previously described dielectric models[1] to lower frequencies and to demonstrate the effectiveness or lack thereof, of several mixture formulas over a wide range of salinities and temperatures.

II. PHYSICAL PROPERTIES OF SEA ICE

Sea ice can be divided into three broad categories by age: young ice, which differs little in structure from first-year ice, but is typically <30 cm thick, first-year ice (30 cm to 2 m thick), and multiyear ice (>2 m thick).

Figure 1 summarizes the properties of first-year ice. It consists of a primary layer of frazil or randomly oriented columnar ice followed by a much thicker layer of large vertically oriented columnar crystals. The salinity of the ice varies from 5 to 16‰ (parts per thousand by weight) near the surface, 4 to 5‰ in the bulk, to approximately 30‰ at the ice-water interface. The density is relatively uniform, 0.92–0.96 g/cm^3, but varies slightly with temperature, salinity, and porosity (see Zubov[17]). Liquid brine is interspersed throughout the ice layer in the form of brine-drainage channels and intercrystalline brine inclusions.[18–21] The average length and radius of the inclusions are 3–5 mm (Poe *et al.*[22]) and 0.025 mm (Pounder[23]), respectively. It is generally assumed that these microscopic brine inclusions are aligned in the growth direction, i.e., they are primarily vertical. This relatively simple structure allows first-year ice to be easily replicated in the laboratory.[1,14,21,24]

Figure 2 summarizes the properties of multiyear ice. The surface of the ice is not smooth; it has undergone an extensive process of recrystallization during the summer melt cycle and consists of an array of refrozen meltponds and hummocks. The upper layer of recrystallized ice, which has a widely varying density (typically 0.7 g/cm^3), merges into a layer of recrystallized ice of slightly higher density, and then into a lower clear-ice layer of density between 0.8 and 0.9 g/cm^3. The salinity of multiyear ice is much lower than that of first-year ice, typically <1‰ near the surface, increasing to 2–3‰ in the bulk (clear ice). This much lower salinity is due to the extensive drainage of brine from the ice during the summer melt period. Unfortunately, the brine-drainage structure of multiyear ice is poorly understood and little has been published describing it.

The brine content and distribution of sea ice has been described by Assur,[25] and polynomial equations have been derived[26,27] from his data which relate the relative fraction of brine by volume in standard sea ice to salinity and temperature. These equations provide a mechanism for comparison of the dielectric properties of various sea-ice samples.

III. MEASUREMENT PROBLEMS

A. Sampling considerations

Probably the most important structural feature of sea ice is the brine inclusion. Because of the high complex-dielectric constant of the liquid brine contained in these inclusions, an ice sample will present a considerable orientation-dependent insertion loss to the measurement system. Therefore, the apparatus should ensure, as much as possible, that the orientation of the electric field with respect to the brine pockets that is encountered *in situ* is reproduced during measurement.

The mechanisms of brine drainage also have significant bearing on measurement procedures. As pointed out by Ad

[a)]Present address: Communications Canada, Cammunications Research Centre, Box 11490, Station H, Shirley Bay, Ottawa, Ontario, Canada K2H 8S2.

 0021–8979/78/4903–1264$01.10

TABLE I. Summary of previous work.

Frequency	Salinity (‰)	Temperature (−°C)	Comments	Author
		Artificial sea ice		
20 Hz to 100 MHz	7–20	22	Special cell used	Addison and Pounder (Refs. 5 and 6)
20 Hz to 100 MHz	4–20	12.5–35	Special cell used, Sillars—dielectric model evaluated	Addison (Refs. 2 and 3)
1 kHz	From saline water 35‰	25–150	Special cell used	Addison *et al.* (Ref. 7)
30, 60, 100, 200, and 400 MHz	0.56, 4.4, 8.6, and 17.0	10–40	Sea water frozen in coaxial air line, poor facsimile	Bogorodsky and Tripol'nikov (Ref. 8)
100 MHz	3.5, 0.7, and 0.35	10–70	...	Cook (Ref. 9)
100 MHz to 24 GHz	6, 8, and 10	0–80	Flash frozen sea water, poor facsimile, conducting spheres, dielectric model	Hoekstra and Cappillino (Ref. 4)
10 GHz	10–60	0–25	NaCl ice	Hoekstra (Ref. 10)
31.4 and 34 GHz	7.8	7	Free-space measurement	Vant *et al.* (Ref. 1)
		Natural sea ice		
100 Hz to 50 kHz	11, 13, and 15	5–70		Fujino (Ref. 11)
0.1–30 MHz	0.067–23	5–40	Possibly severe brine drainage	Wentworth and Cohn (Ref. 12)
150, 300, 500, and 1000 MHz	...	1–60	Very low salinity	Ragle *et al.* (Ref. 13)
100, 200, 400, 800, 1000, 2000, and 4000 MHz	1.32–10.5	5, 10, 15, 20, 25, 30, and 40	Large number of samples	This work and Vant (Ref. 14)
7.5 GHz	4.1–7.5	(as above)	Multiyear and first-year ice, several dielectric models discussed	
10 GHz	0.60–4.4	70–60	Differentiation of ice types, simple dielectric models discussed	Vant *et al.* (Ref. 1)
10 GHz	2.5–7.5	1–13	Good survey of ice types	Bogorodsky and Khokhlov (Ref. 15)
26–40 GHz	2.85, 3.40, and 7.20	7, 16.5, 21.5, 25, and 32		Sackinger and Byrd (Ref. 16)

dison[2,3] and Addison *et al.*,[7] the brine starts to leak from the brine pockets immediately after cutting. This process is especially fast at temperatures above −20 °C. Furthermore,

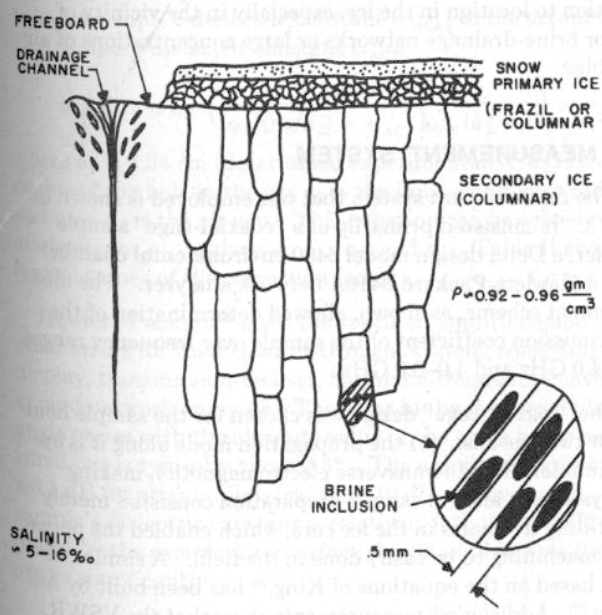

FIG. 1. Simplified geometry of first-year sea ice.

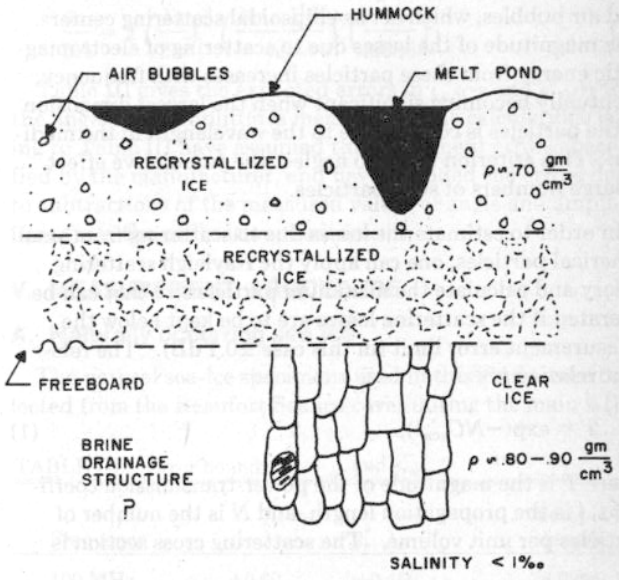

FIG. 2. Simplified geometry of multiyear sea ice.

if brine drainage occurs by the brine expulsion mechanism described by Eide and Martin,[21] then leakage will occur, although moderated, even at lower temperatures.

Small cracks or air gaps in the sample will also affect the

measured dielectric properties, particularly in regions of intense electric fields. Therefore, samples containing such cracks must be rejected. It should be noted, however, that some ice samples, especially those composed of multiyear ice, will necessarily contain many small air bubbles which cannot be ignored in the interpretation. A method of estimating the effects of these bubbles will be discussed in more detail later.

If the samples undergo large temperature fluctuations, recrystallization may also affect their properties. This problem was investigated in a previous paper.[1] It was found that only the sample temperature, not its temperature history during measurement, was important. Furthermore, crystallographic analysis of first-year sea ice which had undergone similar temperature changes to those encountered during measurement showed that no gross alterations in crystal structure occurred. Therefore, it was concluded that as long as no appreciable melting occurred, the measurement procedure employed previously would have no noticeable effect on ice structure.

In summary then, the measurement procedure should (1) involve minimal handling of the specimen, (2) avoid any handling or cutting at temperatures above −20 °C, (3) avoid long periods of sample storage above temperatures of −20 °C, (4) avoid specimens containing cracks, and (5) where possible, use the same specimen and orientation for a series of measurements, e.g., ϵ' and ϵ'' versus frequency, or ϵ' and ϵ'' versus temperature. This last limitation is an attempt to reduce the scatter introduced into the measurement results by variations in the physical properties of the sea ice from location to location.

B. Scattering considerations

Sea ice contains many particles, such as brine inclusions and air bubbles, which act as ellipsoidal scattering centers. The magnitude of the losses due to scattering of electromagnetic energy from these particles increases with frequency, eventually becoming significant when the largest dimension of the particles is comparable to the wavelength in the medium. This criterion tends to neglect the cumulative effect of large numbers of such particles.

In order to estimate the losses due to scattering from small spherical particles, one can apply the Rayleigh scattering theory and calculate the maximum particle size that can be tolerated if the scattering losses are to be kept below the measurement error limit (in this case ±0.1 dB). The relevant relation is[28]

$$T = \exp(-NC_{\text{sca}}l), \tag{1}$$

where T is the magnitude of the power-transmission coefficient, l is the propagation length, and N is the number of particles per unit volume. The scattering cross section is

$$C_{\text{sca}} = (24\pi^3V^2)\lambda^{-4}|(m^2-1)/(m^2+2)|^2, \tag{2}$$

where m is the ratio of the complex refractive index of the particle to that of the medium, λ is the wavelength in the medium, and V is the particle volume.

For an ellipsoid, equivalent values of radius can be found, and the spherical scattering theory can still be employed. The value of equivalent radius (a') is given by

$$(a')^3 = \left(\frac{4}{3}abc\right)(m^2+2)[4\pi + (m^2-1)P_{a,b,\text{ or }c}]^{-1}, \tag{3}$$

where P is the depolarization factor, which is given by

$$P_{b,c} = 4\pi(b/a)^2(1/4e^3)[2e(b/a)^{-2} + \log_e(1-e)/(1+e \tag{4}$$

for the case of the ellipsoid major axis perpendicular to the electric field, and

$$P_a = 4\pi(b/a)^2(1/2e^3)[-2e + \log_e(1+e)/(1-e)] \tag{5}$$

for the case of it parallel to the electric field. The eccentricity

$$e = [1-(b/a)^2]^{1/2} \tag{6}$$

and a and $b = c$, are the ellipsoid semimajor and semiminor axes, respectively.

These equations can be used to calculate a limiting value of λ beyond which scattering losses may be excessive. If the dimensions of the brine ellipsoids are assumed to be $a = 5.0$ mm, and $b = c = 0.025$ mm, and the air bubbles are assumed to be 0.5 mm in radius, in first-year ice, then the limiting value of λ, for end-on incidence of the electric field with respect to the ellipsoids, is 0.28 cm. For multiyear ice with spherical air bubbles of radius 0.5 cm, the limiting value of λ is 7.0 cm.

The number of particles per unit volume N was calculated from the volume fractions and the size of the particles. The volume fractions used in the calculations were 0.11 for brine and 0.015 for air in first-year ice; and 0.244 for air in multiyear ice. Also, nominal values of $70-j20$ and 3.14 were assumed for the dielectric constants of brine and ice, respectively. It should be noted that the value assumed for the complex-dielectric constant of brine is a worst case.

These results indicate that data obtained at frequencies above 24 GHz for first-year ice and above 1.5 GHz for multiyear ice may suffer a certain amount of variation in the measured values due to the inclusion of scattering losses in the measurement. The scattering loss varies greatly from location to location in the ice, especially in the vicinity of major brine-drainage networks or large concentrations of air bubbles.

IV. MEASUREMENT SYSTEM

The measurement system that was employed is shown in Fig. 3. It consisted primarily of a "coaxial-cage" sample holder, a Delta design model 6400 environmental chamber, and a Hewlett-Packard 8410A network analyzer. The measurement scheme, as shown, allowed determination of the transmission coefficient of the sample over frequency ranges 0.1–4.0 GHz and 4.0–8.0 GHz.

The "coaxial-cage" design was chosen for the sample holder for two reasons: (1) the propagation mode along it is approximately TEM (transverse electromagnetic), making analysis easy; and (2) sample preparation consisted merely of drilling five holes in the ice core, which enabled the necessary machining to be easily done in the field. A similar device, based on the equations of King,[29] has been built by Addison.[30] Addison's[30] measurements show that the VSWR (voltage standing wave ratio) of the line can be kept to less

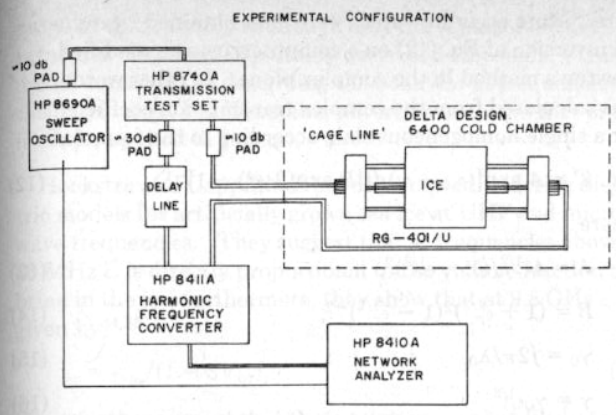

FIG. 3. Wide-band-measurement system employing "coaxial-cage" line; bandwidth, 100 MHz to 7.5 GHz.

than 1.1 for frequencies up to 6.0 GHz and that radiation losses are minimal.

The detailed design of the "coaxial-cage" sample holder used here has been described elsewhere.[14] The transmission line consists of four General Radio silver-plated precision rods 0.24425 in. (0.62040 cm) in diameter which constitute the outer conductors, and a 0.382-in. (0.970-cm)-diam rod which forms the inner conductor. The four outer conductors are equally spaced on a 0.977-in. (2.482-cm)-diam bolt circle surrounding the center conductor. One end of each of the four outer rods is firmly fixed in a brass end block; the other end makes a close sliding fit with a hole in the other end block. The center conductor contains a step transition from 0.382 in. (0.970 cm) to 0.244 in. (0.620 cm) at each end; its position is determined experimentally. This 50–50-Ω step transition is necessary to allow mating with the GR-900-type connector inner conductor.

Because the holes in the ice core must be drilled slightly oversize to allow it to be impaled on the "coaxial-cage" line, there always exists an air gap about each of the conductors. This air gap must be corrected for in the measurements. A semiempirical equation was derived[14] to relate the *measured* relative complex-dielectric constant $\epsilon_{r\,\mathrm{MEAS}}$ to the *actual* relative complex-dielectric constant $\epsilon_{r\,\mathrm{ACT}}$:

$$\epsilon_{r\,\mathrm{MEAS}} = \epsilon_{r\,\mathrm{ACT}} \left(\frac{\log_e(a_3/a_1)}{\log_e(a_3/a_2) + \epsilon_{r\,\mathrm{ACT}} \log_e(a_2/a_1)} \right)^2, \tag{7}$$

where a_3 is 2.54 cm (determined experimentally), a_2 is the radius of the hole in the ice, a_1 is the inner-conductor radius, and $a_2 - a_1$ is the air gap. This equation can be solved numerically for $\epsilon_{r\,\mathrm{ACT}}$, given $\epsilon_{r\,\mathrm{MEAS}}$, a_2, and a_1. Table II gives typical values of the correction factor $\epsilon_{r\,\mathrm{MEAS}}/\epsilon_{r\,\mathrm{ACT}}$ for sea ice.

Hewlett-Packard[31] gives the specified amplitude and angular errors for their total-instrument system, consisting of display, transmission-test set, harmonic-frequency converter, and network analyzer. The error in the measured phase angle varies with the absolute value of the angle being measured but is typically about ±3°. The amplitude error is ±0.1 dB for attenuations less than 10 dB. Providing the sample's dielectric constant is relatively low, the VSWR produced by the sample-air interface should not increase these errors significantly.

An approximate relation between the error in the measured phase angle and the amplitude, and the error in ϵ_r' and ϵ_r'' can be derived. The relation between ϵ_r' and the real and imaginary parts of the propagation constant β and α is given by[32]

$$(\alpha^2 - \beta^2) = (2\pi/\lambda_0)^2 \epsilon_r'. \tag{8}$$

Similarly, ϵ_r'' is related to α and β by

$$\epsilon_r'' = 2(\lambda_0/2\pi)^2 \beta\alpha. \tag{9}$$

For $\alpha \ll \beta, \theta$, the measured phase angle in radians is given by

$$\theta = (\beta_0 - \beta)d,$$

where β_0 is the propagation constant of free space. Therefore, differentiation of ϵ_r' with respect to θ in degrees, gives

$$\frac{\partial \epsilon_r'}{\partial \theta^\circ} = \frac{-2\lambda_0}{360d}\left(1 - \frac{\theta\lambda_0}{360d}\right), \tag{10}$$

where d is the sample length in cm and λ_0 is the free-space wavelength in cm. [In the two extremes of interest for sea ice; $\alpha^2 = 0.21\ (N/m)^2$ versus $\beta^2 = 135.5m^{-2}$ at 200 MHz, and $\alpha^2 = 21.2\ (N/m)^2$ versus $\beta^2 = 21187m^{-2}$ at 4.0 GHz, validating the assumption that $\alpha^2 \ll \beta^2$.]

A similar expression for $\partial\epsilon_r''/\partial A$ is

$$\frac{\partial \epsilon_r''}{\partial A} = 2\left(\frac{\lambda_0}{2\pi}\right)^2 \left(\frac{2\pi(\epsilon_r')^{1/2}}{\lambda_0}\right)\left(\frac{1}{8.686}\right), \tag{11}$$

Table III gives the expected errors in $\epsilon_{r\,\mathrm{ACT}}'$ and $\epsilon_{r\,\mathrm{ACT}}''$ for the angles and amplitudes measured. The calculations leading to Table III have assumed the instrument errors specified by the manufacturer, and have included the errors due to subtractions of the measured values of angle and amplitude from the calibration readings.

TABLE II. Typical air gap correction factors for sea ice (the average gap size encountered was 0.003 in.) ($\epsilon_{r\,\mathrm{ACT}} = 3.4 - j0.165$).

Gap size (in.)	$\epsilon_{r\,\mathrm{MEAS}}'/\epsilon_{r\,\mathrm{ACT}}'$	$\epsilon_{r\,\mathrm{MEAS}}''/\epsilon_{r\,\mathrm{ACT}}''$
0.001	0.988	0.970
0.002	0.971	0.933
0.003	0.954	0.897
0.004	0.936	0.861
0.005	0.928	0.836

V. MEASUREMENT PROCEDURE

A. Naturally occurring sea ice

The natural sea-ice specimens used in this study were collected from the Beaufort Sea ice cover during the main AID-

TABLE III. Error bounds on $\epsilon_{r\,\mathrm{ACT}}'$ and $\epsilon_{r\,\mathrm{ACT}}''$.

Frequency	ϵ_r'	ϵ_r''	Sample length
100 MHz	±0.60	±0.450	8.0 cm
200 MHz	±0.50	±0.230	8.0 cm
400 MHZ	±0.24	±0.100	8.0 cm
800 MHz	±0.17	±0.060	8.0 cm
1.0 GHz	±0.13	±0.045	8.0 cm
2.0 GHz	±0.07	±0.022	8.0 cm
4.0 GHz	±0.03	±0.010	8.0 cm
4.0 GHz	±0.12	±0.045	2.0 cm
7.5 GHz	±0.07	±0.022	2.0 cm

JEX experiment in April 1975. The approximate coordinates of the camp at that time were 76°26′N 140°50′W. The specimens, because of the time of sampling, are representative of winter-spring sea ice.

Ice cores were obtained using a SIPRE ice corer which yielded approximately vertical cores 1 m in length and 7.6 cm in diameter. Salinity and density profiles were determined by sectioning cores into 1-cm-long pieces, using a bandsaw, and then weighing the standard sections to obtain densities, bagging the pieces, melting them, and measuring the salinity of the melt with a standard Beckmann conductivity bridge, calibrated in parts per thousand salt content by weight. The accuracy of the density measurements is estimated at ±0.02 g/cm^3 and the accuracy of the salinity measurements at ±0.2‰. All samples were stored in an unheated building at a temperature of less than −20 °C prior to use.

In order to minimize the effect of scattering of electromagnetic energy from the salinity gradient, the ice samples used for the dielectric measurements were carefully selected from a region of the core having a reasonably flat salinity profile.

Once the sections of the core had been selected they were cut to the desired length and the five holes necessary for mounting on the sample holder were made using a hand drill and a drill jig. All of the machining and fitting of the specimen to the sample holder was done in the unheated building at approximately −20 °C. Preliminary tests showed that, once the sample was placed in the cold chamber, it was necessary to wait approximately 90–100 min for the temperature of the interior of the ice sample to stabilize to within ±0.1 °C of the chamber temperature.

After the sample had reached the desired temperature, its transmission coefficient was measured at frequencies of 0.1, 0.2, 0.4, 0.8, 1.0, 2.0, and 4.0 GHz. The frequencies were accurately set to within ±2 MHz using a digital frequency counter (EIP model 351D). Once a particular set of measurements was finished, the temperature of the chamber was reset and the complete procedure repeated until the sample had been measured at −40, −30, −25, −20, −15, −10, and −5 °C. At the conclusion of the measurements on each sample, it was removed from the chamber, bagged, melted, and its salinity determined. For the higher-frequency tests, the procedure was modified somewhat by using shorter samples, approximately 2 cm in length, and measuring them at 4.0 and 7.5 GHz.

Density measurements were not performed on the actual samples themselves. The only worthwhile density measurement that could have been performed on the samples themselves would require use of the immersion technique. It was feared that this technique would contaminate the specimens if done prior to measurement, and would contaminate the salinity measurement if done afterwards. For the above reasons, it was decided to rely solely on density data from adjacent cores. Since the samples were almost all young or first-year ice, this technique yielded reasonably representative figures for density, although it may have contributed somewhat to the scatter of the data.

The transmission-coefficient data obtained using the foregoing procedure were referenced to the transmission coefficient for the empty sample holder, and then analyzed to a first-order approximation at the site using a graphical procedure. More accurate values were later obtained by numerical inversion of Eq. (12) on a computer, using a modified Newton's method in the complex plane. In other words, ϵ_r was calculated from the complex transmission coefficient T for a single homogeneous slab, according to the formula[33]

$$T = A \exp[(\gamma_0 - \gamma)d][B \exp(2\gamma d) - 1]^{-1}, \tag{12}$$

where

$$A = 4\epsilon_r^{1/2}/(1 - \epsilon_r^{1/2})^2, \tag{13}$$

$$B = (1 + \epsilon_r^{1/2})^2(1 - \epsilon_r^{1/2})^{-2}, \tag{14}$$

$$\gamma_0 = j2\pi/\lambda_0, \tag{15}$$

$$\gamma = \gamma_0 \epsilon_r^{1/2}. \tag{16}$$

ϵ_r is the complex relative dielectric constant, λ_0 is the free-space wavelength in cm, and d is the length of the sample in cm.

B. Artificial sea ice

Artificial sea-ice specimens were grown in the laboratory using a suitable method.[1,24] Vertical slabs were cut and smaller samples were removed from these slabs at angles of 0°, 30°, 45°, 60°, and 90° to the vertical. These specimens were mounted on the "coaxial-cage" line so that the normal vertical direction was at the above-mentioned angles to the direction of wave propagation. Measurements were performed on the samples at −40, −25, −15, −10, −8, and −6 °C over the frequencies 0.1, 0.2, 0.4, 0.8, 1.0, 2.0, and 4.0 GHz using the technique described in Sec. V A.

VI. DIELECTRIC MODELS AND EXPERIMENTAL RESULTS

A. Background

To describe the dielectric behavior of saline ice in the MHz frequency region, Addison[3] has employed the Maxwell-Wagner-Sillars equations:

$$\epsilon_r' = \epsilon_{r\infty}' + \epsilon_{r\infty\mathrm{ice}}' N(1 + \omega^2\tau_s^2)^{-1},$$

$$\epsilon_r'' = \epsilon_{r\infty\mathrm{ice}}' N\omega\tau_s(1 + \omega^2\tau_s^2)^{-1},$$

$$\tau_s = \epsilon_0\{[\epsilon_{r\infty\mathrm{ice}}'(n-1) + \epsilon_{r\mathrm{br}}']/\sigma_{\mathrm{br}}\},$$

$$N = V_{\mathrm{br}}\{n^2\epsilon_{r\infty\mathrm{ice}}'[\epsilon_{\infty\mathrm{ice}}'(n-1) + \epsilon_{\mathrm{br}}']^{-1}\}, \tag{17}$$

where $\epsilon_{r\infty}' \simeq \epsilon_{r\infty\mathrm{ice}}'$. Here, n is a function of a/b and has the values

$$a/b < 1, \qquad n \sim 1,$$

$$a = b(\text{sphere}), \qquad n = 3,$$

$$a \gg b(\text{long prolate}), \qquad n \sim (a^2/b^2)[\ln(2a/b) - 1]^{-1}, \tag{18}$$

and V_{br} is the fraction of volume occupied by the brine, which may be calculated using the equations of Frankenstein and Garner[26] and Poe *et al.*,[27] or the data of Assur.[25] The relaxation time Addison calculated using these equations is too short; however, by using empirical determinations of relaxation spectra he succeeded in obtaining a more suitable relaxation time, corresponding to a relaxation effect in the vicinity of 50 MHz. By assigning a value of 50 to a/b, he calculated an ϵ_r' and ϵ_r'' which were roughly four times too large in comparison with his experimental data at 50 MHz. From this he concluded that the Sillar's model was appropriate,

but that the ice acted as though only one-quarter of the brine was contained in suitably described ellipsoids. This model succeeded in describing the behavior at frequencies in the MHz range, but it remains uncertain as to whether or not it can be applied in general.

Hoekstra and Cappillino[4] have attempted to derive dielectric models for artificially grown sea ice at UHF and microwave frequencies. They suggest that at frequencies above 10 MHz ϵ_r'' is directly proportional to the volume fraction of brine in the ice; furthermore, they show that at 9.8 GHz ϵ_r' is given by[34,35]

$$\epsilon_r' = \epsilon_{r\text{ice}}'/(1 - 3V_{\text{br}}). \tag{19}$$

They further suggest that these relations are not likely to be accurate at lower frequencies where interfacial effects, the mechanisms responsible for the mixture behavior, play a lesser role.

Previous work by the authors,[1] on natural sea ice, has also shown that, at 10 GHz, ϵ_r' is indeed linearly related to $1/(1 - 3V_{\text{br}})$, although the relation is not exact.

Instead,

$$\epsilon_r' = a_0 + a_1(1 - 3V_{\text{br}})^{-1}. \tag{20}$$

Linear correlations showed that the best fits to the data for three types of sea ice (columnar grained first year, frazil grained first year, and multiyear) were obtained for $a_0 \neq 0$ and $a_1 \neq 3.14$. This suggests that all the brine is not in the form of spherical inclusions, but that perhaps a more exact model assuming elliptical inclusions at some angle to the electrical field might hold.

A linear correlation[1] of the ϵ_r'' data with V_{br} showed that ϵ_r'' is directly related to V_{br}, although the correlation coefficients obtained (0.723–0.849) do not exclude other interpretations.

A second model for ϵ_r', based on the Weiner dielectric mixture formula,[36] was also tested.[1] This model allows a more general particle shape—anything from spheres to lamellae. It was found that, at 10 GHz, a model of this form accurately described the dielectric behavior of frazil first-year ice and to a certain extent multiyear ice.

The above models indicate that simple mixture formulas can, at least at 10 GHz, and other single frequencies or narrow bands of frequencies, adequately describe the dielectric behavior of sea ice. Whether or not such models are widely applicable has yet to be determined.

deLoor[34] has listed the various effects which can contribute to the average dielectric constant of mixtures containing water. These effects are charged double-ion layers (active in the frequency range 10^0–10^5 Hz), dc conductivity (10^0–10^9 Hz), ice relaxation (10^2–10^4 Hz), Maxwell/Wagner losses (10^2–10^6 Hz), crystal water relaxation (10^1–10^4 Hz), surface conductivity (10^3–10^9 Hz), bound forms of water relaxation (10^6–10^9 Hz), and water relaxation (10^9–10^{11} Hz). The magnitude of surface conductivity and bound water-relaxation effects in sea ice are not known.

Addison[3] has more specifically identified the major mechanisms contributing to the observed dielectric properties of sea ice. These are (high-frequencies) Maxwell-Wagner-Sillars dispersion, (mid-frequencies) Debye dispersion of the ice protons with reduced relaxation time, and (low-frequencies) dispersion resulting from ion-space charge polarization in the brine channels.

It is these effects that will ultimately determine the behavior of the sea-ice mixture. Many dielectric mixture formulas have been derived[35] for specific geometries, concentrations, and frequency ranges of applicability. Section IV B investigates the applicability of several of these formulas.

B. Empirical models

Many of the dielectric mixture formulas mentioned previously[35] have the form

$$\epsilon_r' = a_0 + a_1 V_{\text{br}}. \tag{21}$$

To test the formulas of this form, the data for both ϵ_r' and ϵ_r'' were first linearly correlated against the relative volume fraction of brine. Table IV gives the successful ϵ_r', ϵ_r'', and loss linear correlations. The data was gathered from 11 first-year sea-ice samples having salinities in the range 4.1–10.5 ± 0.2‰, and densities equal to 0.91 ± 0.02 g/cm^3; two multiyear ice samples of salinity 1.32 ± 0.05 and 1.75 ± 0.05‰, and density 0.905 ± 0.01 and 0.903 ± 0.01 g/cm^3; and 10 samples of artificial sea ice having salinities in the range from 3.0 ± 0.2 to 3.9 ± 0.2‰, and densities of 0.90 ± 0.02 g/cm^3.

The first group of data in Table IV shows the results of the correlation of ϵ_r' with V_{br} for the first-year ice samples over the frequency range 0.1–4.0 GHz. It is apparent that all the r^2 values are between 0.71 and 0.76, thereby indicating that the correlation is reasonably good. Comparison of the standard errors s_{yx} and the error bounds $\pm\Delta$ shows that the error bounds are larger than the standard errors at the lower frequencies, but smaller than the standard errors at the higher frequencies. This implies two things: first, that the natural variability in the sea ice is the prime contributor to s_{yx} at the higher frequencies; and second, that the measurement errors mask some of the underlying behavior at the lower frequencies. A further check with the raw data suggested that there indeed may be a greater variation of ϵ_r' with brine volume at the lower frequencies, but that the true extent of this variation is obscured by the measurement errors.

The next group of data in Table IV shows the results of the correlation for ϵ_r'' versus V_{br}. The standard errors once again show a trend of steadily decreasing value as the frequency increases, then a levelling off to about 0.05 at 4.0 GHz. These standard errors compare with the measurement errors, given in Table III, in much the same manner as the ϵ_r' errors did, i.e., the standard errors are smaller than the measurement errors at the low frequencies but they become three or four times larger than the measurement errors at 4.0 GHz. In general, ϵ_r'' is higher at the low frequencies, decreases with increasing frequency, and exhibits reasonably linear variation with V_{br}. There also appears to be a levelling off of ϵ_r'' with increasing frequency to a value of approximately 0.3–0.4 at $V_{\text{br}} = 1.0$.

At 7.5 GHz ϵ_r'', unlike its ϵ_r' counterpart, shows a good correlation with V_{br}. This implies there is a stronger relation between ϵ_r'' and V_{br} than between ϵ_r' and V_{br}. The extension of the ϵ_r'' correlations to multiyear ice tends to support this hypothesis. The ϵ_r'' points correlate well with V_{br} whereas the ϵ_r' points do not.

TABLE IV. Correlation data for the empirical model based on the AIDJEX measurements. $\hat{y} = a_0 + a_1 V_{br}$, $\hat{y}$ is the estimate of the parameter considered, V_{br} is the calculated brine volume × 10, n is the number of points considered, a_0 is the $\hat{y}$ intercept, a_1 is the slope, r^2 is the coefficient of determination, s_{yx} is the standard error of the estimate ($\hat{y}$), $s_{0,1}$ are the standard errors of $a_{0,1}$, and $\pm\Delta$ is the error bound on the individual points in the sample. The average density of all samples was 0.91 ± 0.03 g/cm^3.

Parameter	Freq. (GHz)	n	a_0	a_1	r^2	s_{yx}	s_0	s_1	$\pm\Delta$
ϵ_r'	0.100	43	3.22	2.06	0.76	0.29	0.07	0.19	0.60
(first year)	0.200	43	3.23	1.45	0.74	0.21	0.05	0.12	0.50
	0.400	37	3.26	1.23	0.74	0.18	0.05	0.12	0.24
	0.800	44	3.12	0.99	0.74	0.15	0.03	0.08	0.17
	1.000	46	3.12	0.90	0.72	0.14	0.02	0.07	0.13
	2.000	47	3.07	0.76	0.72	0.12	0.02	0.06	0.07
	4.000	47	3.05	0.72	0.71	0.12	0.02	0.06	0.03
ϵ_r''	0.100	43	0.161	1.324	0.70	0.212	0.054	0.135	0.450
(first year)	0.200	43	0.043	0.895	0.74	0.132	0.040	0.091	0.230
	0.400	37	0.043	0.715	0.73	0.109	0.033	0.074	0.100
	0.800	44	0.048	0.534	0.80	0.067	0.017	0.041	0.600
	1.000	46	0.039	0.504	0.81	0.061	0.015	0.037	0.045
	2.000	47	0.034	0.356	0.86	0.036	0.008	0.021	0.022
	4.000	47	0.024	0.329	0.77	0.045	0.010	0.027	0.010
	7.50	21	0.032	0.353	0.70	0.051	0.020	0.054	0.022
Loss	0.100	43	0.97	5.11	0.63	0.97	0.25	0.62	
(first year)	0.200	43	0.92	7.00	0.69	1.15	0.37	0.81	
	0.400	37	1.24	11.96	0.69	1.99	0.60	1.35	
	0.800	44	2.35	19.00	0.77	2.61	0.66	1.61	
	1.000	46	2.38	22.69	0.79	2.92	0.70	1.77	
	2.000	47	3.97	32.92	0.84	3.55	0.83	2.12	
	4.000	47	6.49	60.46	0.75	8.70	2.06	5.21	
	7.50	21	13.37	136.98	0.68	20.02	7.82	21.35	
ϵ_r'	0.100	5	0.022	0.666	0.83	0.033	0.022	0.173	0.450
(multiyear)	0.400	5	−0.058	1.201	0.90	0.034	0.033	0.253	0.100
	0.800	8	0.000	0.474	0.92	0.012	0.006	0.058	0.600
	1.000	10	−0.004	0.436	0.91	0.010	0.005	0.048	0.045
	2.000	13	0.013	0.435	0.73	0.016	0.007	0.080	0.022
	4.000	9	−0.007	0.299	0.91	0.006	0.004	0.036	0.010
Loss	0.100	5	0.12	3.32	0.83	0.15	0.10	0.74	
(multiyear)	0.400	5	−1.17	24.31	0.90	0.69	0.66	4.74	
	0.800	8	−0.02	19.68	0.92	0.49	0.26	2.42	
	1.000	10	−0.27	22.77	0.91	0.49	0.26	2.50	
	2.000	13	1.32	45.66	0.74	1.68	0.77	8.19	
	4.000	9	−1.65	63.68	0.91	1.33	0.86	7.70	

Also given in Table IV are the correlations of the loss in (dB/m) with V_{br}, calculated using[32]

$$\text{loss(dB/m)} = 868.6(2\pi/\lambda_0)\{(\epsilon_r'/2)[(1+\tan^2\delta)^{1/2}-1]\}^{1/2}, \quad (22)$$

where λ_0 is the free-space wavelength in cm, and $\tan\delta = \epsilon_r''/\epsilon_r'$. The results of the correlation show that the loss increases dramatically with frequency. For $V_{br} = 0.9$, the loss is only about 5–6 dB/m for first-year sea ice at 100 MHz, but it increases to approximately 125 dB/m at 7.5 GHz. The slopes relating loss and V_{br} also increase dramatically from 5.11 at 100 MHz to 136.98 at 7.5 GHz, so that at 100 MHz a large brine volume, say $V_{br} = 1.0$, may only increase the loss from its $V_{br} = 0$ value by approximately 5 dB/m, whereas at 7.5 GHz it may increase the loss by as much as 123 dB/m. That is a difference of almost 120 dB for one-way propagation through 1 m of first-year sea ice.

The standard errors for the loss correlations are relatively high. This reflects the combined effect of the errors in ϵ_r' and the errors in ϵ_r'', both of which must be used to calculate the loss.

Comparison of the loss-vs.-V_{br} correlations for multiyear and first-year sea ice shows that the correlations of loss with V_{br} produce lines of almost exactly the same slope for both first-year and multiyear sea ice. This infers that although the absolute losses are lower in multiyear ice due to its lower salinity, the rate of variation of loss with brine-volume fraction is the same in both cases.

Table V presents the results of a linear correlation of the ϵ_r' and ϵ_r'' data for artificial sea ice with the relative brine-volume fraction V_{br}.

The five angles at which samples were taken from the artificial sea-ice sheet have been collected into three groups: 0°, 30°, and 45°-60° and 90°. The lumping of the 45°, 60°, and 90° data was done because there appears to be no significant difference between the data points for each angle, i.e., a 45° data point at the same brine volume gives, within the scatter of the data, the same value for ϵ_r' and ϵ_r'' as a 60° or 90° data point, and so on.

The general trend in the data seems to indicate that the measured values of both ϵ_r' and ϵ_r'' increase, with the sample offset angle from the vertical, up to a maximum, lying somewhere in the range of values given by the 45°-60°-90° line. It cannot be said for certain from this data whether a decrease subsequently occurs.

TABLE V. Correlation data for the empirical model based on the artificial sea-ice measurements. $\hat{y} = a_0 + a_1 V_{br}$, $\hat{y}$ is the estimate of the parameter considered, V_{br} is the calculated brine volume × 10, n is the number of points considered, Angle is the sample taken at this angle, with respect to the vertical, a_0 is the $\hat{y}$ intercept, a_1 is the slope, r^2 is the coefficient of determination, s_{yx} is the standard error of the estimate ($\hat{y}$), $s_{0,1}$ are the standard errors of $a_{0,1}$, and $\pm\Delta$ is the error bound on the individual points in the sample. The average density of all samples was 0.90 ± 0.03 g/cm³.

Parameter	Freq. (GHz)	Angle (deg)	n	a_0	a_1	r^2	s_{yx}	s_0	s_1	$\pm\Delta$
ϵ_r'	0.13	0	13	2.48	3.04	0.68	0.19	0.13	0.65	0.60
		30	14	2.46	4.90	0.81	0.21	0.12	0.69	
		45,60,90	42	2.48	5.60	0.85	0.22	0.08	0.42	
	0.21	0	14	2.95	2.31	0.85	0.10	0.06	0.29	0.50
		30	11	2.94	3.91	0.86	0.12	0.08	0.53	
		45,60,90	34	2.99	4.06	0.86	0.15	0.05	0.29	
	0.45	0	11	2.88	1.72	0.81	0.06	0.06	0.28	0.24
		30	13	2.99	2.11	0.91	0.06	0.04	0.20	
		45,60,90	29	2.95	2.71	0.88	0.09	0.04	0.20	
	0.81	0	11	3.10	1.52	0.71	0.07	0.07	0.33	0.17
		30	12	3.15	1.82	0.83	0.07	0.05	0.25	
		45,60,90	32	3.17	2.11	0.82	0.09	0.03	0.18	
	1.00	0	11	3.14	1.24	0.69	0.06	0.06	0.28	0.13
		30	12	3.21	1.49	0.85	0.06	0.03	0.19	
		45,60,90	29	3.20	1.94	0.81	0.08	0.04	0.18	
	2.01	0	11	3.13	0.78	0.75	0.04	0.03	0.13	0.07
		30	13	3.13	1.06	0.86	0.04	0.02	0.13	
		45,60,90	33	3.12	1.47	0.79	0.07	0.03	0.14	
	4.00	0	14	3.12	0.61	0.80	0.03	0.02	0.09	0.03
		30	14	3.09	0.95	0.88	0.03	0.02	0.10	
		45,60,90	33	3.12	1.16	0.64	0.08	0.03	0.16	
ϵ_r''	0.13	0	13	0.326	1.03	0.08	0.31	0.21	1.03	0.45
		30	14	0.538	1.49	0.16	0.30	0.17	0.99	
		45,60,90	42	0.236	3.35	0.61	0.25	0.09	0.47	
	0.21	0	14	0.141	1.11	0.34	0.15	0.09	0.45	0.23
		30	11	0.329	0.84	0.13	0.17	0.11	0.73	
		45,60,90	34	0.282	1.70	0.49	0.18	0.06	0.31	
	0.45	0	11	0.162	0.26	0.07	0.07	0.07	0.33	0.10
		30	13	0.157	0.78	0.51	0.07	0.04	0.23	
		45,60,90	29	0.139	2.61	0.57	0.22	0.08	0.44	
	0.81	0	11	0.121	0.55	0.35	0.06	0.06	0.25	0.06
		30	13	0.045	1.32	0.73	0.06	0.04	0.24	
		45,60,90	31	0.062	1.34	0.69	0.08	0.03	0.17	
	1.00	0	11	0.068	0.66	0.55	0.04	0.04	0.20	0.045
		30	13	0.030	1.07	0.75	0.06	0.03	0.19	
		45,60,90	30	0.011	1.30	0.61	0.09	0.04	0.20	
	2.01	0	14	0.029	0.38	0.65	0.03	0.02	0.08	0.022
		30	13	0.054	0.40	0.66	0.03	0.02	0.09	
		45,60,90	33	0.038	0.73	0.68	0.05	0.02	0.09	
	4.00	0	14	0.005	0.48	0.88	0.02	0.01	0.05	0.010
		30	14	0.050	0.54	0.81	0.02	0.01	0.07	
		45,60,90	33	0.025	0.63	0.72	0.03	0.01	0.07	

The general increase, with deviation from the vertical, tends to suggest the brine network has a primarily vertical structure, which is usually aligned almost perpendicular to the electric field. As the samples are tilted, the brine network couples more and more strongly to the field—hence, the increase in ϵ_r' and ϵ_r''.

A comparison of the slopes (a_1 values) given in Table V with those in Table IV shows that for the same frequency, the vertical (0°) samples of artificial sea ice and the natural first-year-ice samples exhibit substantially the same ϵ_r' and ϵ_r'' values. (Differences in the intercept value tend to obscure the similarity in some cases.) This finding suggests that truly representative studies of the dielectric properties of first-year sea ice may be done using laboratory-grown sea-ice sheets. It should also be noted that the a_0 values for the ϵ_r' correlations should in all cases equal 3.14, the dielectric constant of pure ice. It can be seen from Tables IV and V that within the experimental error, this is indeed the case in all but two instances.

It cannot be concluded from these results that a linear-correlation model is the best or the only possible one—the correlation coefficients are not high enough to support such an hypothesis. In view of this, three other simple correlation models were tested. One of these, the $y = a\exp(bx)$ model, is similar to the familiar logarithmic mixture formula suggested by von Hippel.[37] The results of these correla-

TABLE VI. Correlation of experimental data with various mixture models. r^2 is the correlation coefficient, a and b provide the best fit in the least-squares sense, and $x = . V_{br}$.

Model	Ice type	Freq. (GHz)	a	b	r^2	Sample size
$\epsilon_r' = ax^b$	First year	0.100	6.74	0.15	0.75	43
		1.00	4.34	0.07	0.61	46
		4.00	3.98	0.05	0.55	47
	Multiyear	0.100	3.73	0.04	0.82	5
		1.00	3.18	0.01	0.11	10
		4.00	2.98	0.00	0.01	9
$\epsilon_r'' = ax^b$	First year	0.100	10.00	0.86	0.45	43
		1.00	4.04	0.89	0.65	46
		4.00	4.50	1.02	0.64	47
	Multiyear	0.100	4.46	0.83	0.77	5
		1.00	1.06	0.75	0.73	10
		4.00	97.42	1.86	0.61	9
$\epsilon_r' = a + b \ln x$	First year	0.100	6.07	0.59	0.72	43
		1.00	4.26	0.23	0.60	46
		4.00	5.44	0.55	0.56	47
	Multiyear	0.100	3.68	0.11	0.81	5
		1.00	3.18	0.02	0.11	10
		4.00	2.98	−0.01	0.01	9
$\epsilon_r'' = a + b \ln x$	First year	0.100	1.24	0.19	0.25	43
		1.00	0.68	0.13	0.68	46
		4.00	0.44	0.08	0.68	47
	Multiyear	0.100	0.24	0.03	0.86	5
		1.00	0.15	0.02	0.59	10
		4.00	0.19	0.04	0.94	9
$\epsilon_r' = a \exp(bx)$	First year	0.100	3.26	5.10	0.73	43
		1.00	3.13	2.57	0.73	46
		4.00	3.06	2.14	0.69	47
	Multiyear	0.100	2.94	5.40	0.91	5
		1.00	3.09	0.10	0.01	10
		4.00	3.01	−0.06	0.00	9
$\epsilon_r'' = a \exp(bx)$	First year	0.100	0.17	27.21	0.39	43
		1.00	0.06	28.89	0.53	46
		4.00	0.04	23.14	0.35	47
	Multiyear	0.100	0.02	101.29	0.55	5
		1.00	0.01	119.87	0.82	10
		4.00	0.00	149.96	0.51	9

tions, given in Table VI, show that of the four correlation models presented thus far, the linear model is the best.

A correlation of the form given in Eq. (20) was also performed on the data. The results are shown in Table VII. Note that the agreement is reasonably good over the whole frequency range 0.1–7.5 GHz, for both ϵ_r' and ϵ_r''. However, as found previously at 10 GHz,[1] $a_0 \neq 0$ and a_1 is not exactly 3.14.

C. Theoretical model

The above correlations represent an attempt to find a suitable form for the equation describing the mixture dielectric constant. Many other equations also exist,[34,35,38,39] but a survey of the literature showed that one due to Tinga *et al.*[39] may have particular promise. Their work was directed towards the prediction of the dielectric constant of various concentrated solutions containing water. Preliminary calculations tended to indicate that it might also apply to sea-ice mixtures. The mixture dielectric constant ϵ_{AV} is given by

$$\frac{\epsilon_{AV} - \epsilon_1}{\epsilon_1} = \frac{V_2}{V_1} \frac{\epsilon_2 - \epsilon_1}{[-(V_2/V_1)n_1(\epsilon_2 - \epsilon_1) + n_2(\epsilon_2 - \epsilon_1) + \epsilon_1]}, \quad (23)$$

where V_1 and V_2 are the volume fractions of the host medium and inclusion, respectively, and n_1 and n_2 are the depolarization ceofficients. In the case of interest, i.e., ellipsoidal inclusions, the n_1 and n_2 are equal and are given by[28]

$$n_1^{b,c} = \left(\frac{b}{c}\right)^2 \left(\frac{1}{4e^3}\right) \left(\frac{2e}{(b/a)^2} + \log_e \frac{(1-e)}{(1+e)}\right) \quad b = c \quad (24)$$

and

$$n_1^a = (b/a)^2 \left(\frac{1}{2e^3}\right) \left(-2e + \log_e \frac{(1+e)}{(1-e)}\right) \quad a > b, \quad (25)$$

where the a, b, and c refer to the elipsoid axis along which the electric field is applied and e is the ellipsoid eccentricity defined by

$$e = [1 - (b/a)^2]^{1/2}. \quad (26)$$

For spherical inclusions, $n_1^{a,b,c} = \frac{1}{3}$.

TABLE VII. Correlation of experimental data with conducting spheres model.

Model	Ice types	Freq. (GHz)	a_0	a_1	r^2	Sample size
$\epsilon_r' = a_0 + \frac{a_1}{1-3x}$	First year	0.100	−1.42	4.75	0.72	43
		0.200	−0.03	3.33	0.77	37
		0.400	0.45	2.89	0.78	37
		0.800	0.83	2.33	0.73	44
		1.00	1.01	2.15	0.74	46
		2.00	1.28	1.82	0.72	47
		4.00	1.35	1.73	0.71	47
$\epsilon_r'' = a_0 + \frac{a_1}{1-3x}$	First year	0.100	−2.85	3.08	0.68	43
		0.200	−1.93	2.03	0.73	37
		0.400	−1.54	1.63	0.73	37
		0.800	−1.17	1.25	0.78	44
		1.00	−1.12	1.18	0.79	46
		2.00	−0.78	0.83	0.82	47
		4.00	−0.73	0.77	0.75	47
		7.50	−0.79	0.84	0.66	21
	Multiyear	0.100	−2.05	2.08	0.83	5
		0.400	−3.99	3.93	0.91	5
		0.800	−1.51	1.51	0.92	8
		1.00	−1.37	1.37	0.92	10
		2.00	−1.33	1.35	0.72	13
		4.00	−0.95	0.94	0.91	9

Equation (23) can be used to calculate the complex-dielectric constant of a mixture providing the quasistatic assumption is met,[14] i.e., scattering effects are minimal. By previous calculation this would limit the model applicability to frequencies less than 24 GHz for first-year ice and 1.5 GHz for multiyear ice.

As previously expressed, Eq. (23) can be used to calculate the dielectric constant of mixtures containing ellipsoids oriented either parallel or perpendicular to the electric vector of the probing wave. For waves applied at other angles, it is assumed that for the horizontally (perpendicular) polarized component of the wave the dielectric constant is always $\epsilon_{AV,b}$ irregardless of angle, and that for the vertically (parallel) polarized component, the equivalent dielectric constant is given by[40]

$$\frac{1}{\epsilon_{AV,\theta}} = \frac{\sin^2\theta}{\epsilon_{AV,a}} + \frac{\cos^2\theta}{\epsilon_{AV,b}}, \tag{27}$$

where θ is the angle between the a axis and the direction of propagation. For the geometry shown in Fig. 4, illuminated by a normally incident randomly oriented in-azimuth electromagnetic plane wave, the complex-dielectric constants for vertical and horizontal polarization contribute equally to the effective dielectric constant.[14] Thus,

$$\epsilon_{\text{eff}} = \tfrac{1}{2}\epsilon_{AV,b} + \tfrac{1}{2}\epsilon_{AV,\theta}. \tag{28}$$

To obtain the mixture dielectric constant for sea ice, Eqs. (23)–(28) must be applied twice, once to calculate the effect of the ellipsoidal brine inclusions and once to calculate the effect of the spherical air bubbles. However, before these calculations can be made the dielectric constants for both brine and pure ice must be known.

Stogryn[41] has presented a reasonable dielectric model for brine, but only for certain combinations of concentration and temperature. His model is primarily an amalgamation of several previously published measurements into a single set of empirical equations.

His model assumes that the complex dielectric constant of the brine can be adequately represented by an equation of the Debye form

$$\epsilon_{r_{\text{br}}} = \epsilon_{r_{\infty\text{br}}} + \frac{\epsilon_{r_{0\text{br}}} - \epsilon_{r_{\infty\text{br}}}}{1 + j\omega\tau_{\text{br}}} - \frac{j\sigma_{\text{br}}}{\epsilon_0\omega}, \tag{29}$$

where $\epsilon_{r_{0\text{br}}}$ and $\epsilon_{r_{\infty\text{br}}}$ are, respectively, the static and high-frequency dielectric constants of the solvent (modified by the solute), τ_{br} is the relaxation time of the brine in seconds, ϵ_0 is the permittivity of free space (-8.854×10^{-12} F/m), σ_{br} is the ionic conductivity of the dissolved salts in mho/m, and ω is the radian frequency.

To obtain values for the various parameters in Eq. (29), Stogryn[41] has fit the available dielectric data[42–46] to simple polynomial equations. He gives $\epsilon_{r_{0\text{br}}}$ as

$$\epsilon_{r_{0\text{br}}}(T,N) = \epsilon_{r_{0\text{br}}}(T,O)a(N), \tag{30}$$

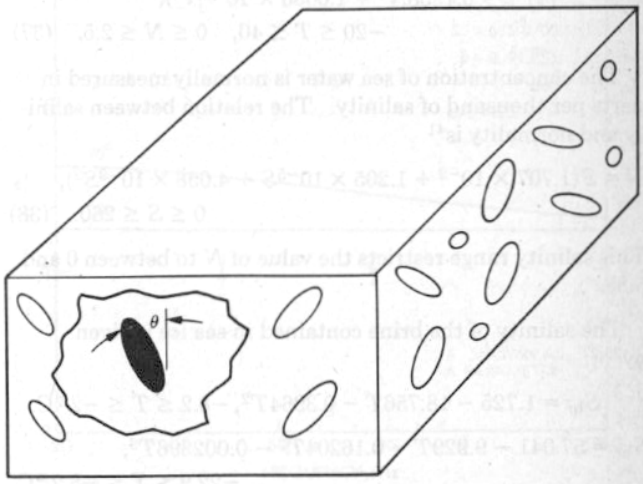

FIG. 4. Conceptual view of ellipsoid model; all ellipsoids are assumed to lie at angle θ with respect to the vertical, but can have arbitrary azimuthal orientation.

where T is the temperature in °C, N is the normality of the solution, $a(N)$ (for NaCl) is

$$a(N) = 1.000 - 0.2551N + 5.151 \times 10^{-2}N^2 - 6.889 \times 10^{-3}N^3, \quad 0 \le T \le 40\ °C, 0 \le N \le 3, \quad (31)$$

and

$$\epsilon_{r0\mathrm{br}}(T,O) = 87.74 - 0.4008T + 9.398 \times 10^{-4}T^2 - 1.410 \times 10^{-6}T^3. \quad (32)$$

Similarly,

$$2\pi\tau_{\mathrm{br}}(T,N) = 2\pi\tau_{\mathrm{br}}(T,O)b(N,T), \quad (33)$$

where $\tau_{\mathrm{br}}(T,O)$ is given by

$$2\pi\tau_{\mathrm{br}}(T,O) = 1.1109 \times 10^{-10}T^2 - 3.824 \times 10^{-12}T + 6.938 \times 10^{-14}T^2 - 5.096 \times 10^{-16}T^3 \quad (34)$$

and

$$b(N,T) = 0.1463 \times 10^{-2}NT + 1.000 - 0.04896N - 0.0296N^2 + 5.644 \times 10^{-3}N^3, \quad 0 \le T \le 40\ °C, \quad 0 \le N \le 3. \quad (35)$$

A value of 4.9 has been assumed for $\epsilon_{r\infty\mathrm{br}}$, which according to Stogryn[41] affords the best fit to the published experimental data. He also states that there is no evidence to suggest $\epsilon_{r\infty\mathrm{br}}$ depends on salinity. Therefore, the value for pure water was used and any slight variations with temperature were ignored.

Obviously, pure nonsupercooled water turns to ice below 0 °C, therefore, Eqs. (32) and (34) do not hold at temperatures below 0 °C. This represents a rather unsatisfactory element of the brine model. However, it is expected that as long as the brine is liquid, extrapolations of Eqs. (30)–(35) should represent a reasonable first approximation.

The remaining parameter σ_{NaCl} is given by

$$\sigma_{\mathrm{NaCl}}(T,N) = \sigma_{\mathrm{NaCl}}(25,N)\{1.000 - 1.962 \times 10^{-2}\Delta + 8.08 \times 10^{-5}\Delta^2 - \Delta N[3.020 \times 10^{-5} + 3.922 \times 10^{-5}\Delta + N(1.721 \times 10^{-5} - 6.584 \times 10^{-6}\Delta)]\}, \quad (36)$$

where $\Delta = 25 - T$, and

$$\sigma_{\mathrm{NaCl}}(25,N) = N(10.394 - 2.3776N + 0.68258N^2 - 0.1358N^3 + 1.0086 \times 10^{-2}N^4), \quad -20 \le T \le 40, \quad 0 \le N \le 2.5. \quad (37)$$

The concentration of sea water is normally measured in parts per thousand of salinity. The relation between salinity and normality is[41]

$$N = S(1.707 \times 10^{-2} + 1.205 \times 10^{-5}S + 4.058 \times 10^{-9}S^2), \quad 0 \le S \le 260. \quad (38)$$

This salinity range restricts the value of N to between 0 and 5.35.

The salinity of the brine contained in sea ice is given by[25,27]

$$S_{\mathrm{br}} = 1.725 - 18.756T - 0.3964T^2, \quad -8.2 \le T \le -2\ °C,$$

$$S_{\mathrm{br}} = 57.041 - 9.929T - 0.16204T^2 - 0.002396T^3, \quad -22.9 \le T \le -8.2\ °C,$$

$$S_{\mathrm{br}} = 242.94 + 1.5299T + 0.0429T^2, \quad -36.8 \le T \le -22.9\ °C,$$

$$S_{\mathrm{br}} = 508.18 + 14.535T + 0.2018T^2, \quad -43.2 \le T \le -36.8\ °C. \quad (39)$$

These equations agree well with the experimental data of Zubov[17] only at temperatures above approximately −12 °C.

Considerable dielectric information exists for pure ice.[47] For the purpose of the sea-ice model, pure ice will be assumed to be a Debye substance with $\epsilon'_{r\mathrm{ICE}}$ given by[48]

$$\epsilon'_{r\mathrm{ICE}} = \epsilon'_{r\infty\mathrm{ICE}} + \frac{\epsilon'_{r0\mathrm{ICE}} - \epsilon'_{r\infty\mathrm{ICE}}}{1 + \omega^2\tau^2_{\mathrm{ICE}}} \quad (40)$$

and

$$\epsilon''_{r\mathrm{ICE}} = \frac{\epsilon'_{r0\mathrm{ICE}} - \epsilon'_{r\infty\mathrm{ICE}}}{1 + \omega^2\tau^2_{\mathrm{ICE}}}\omega\tau_{\mathrm{ICE}}, \quad (41)$$

where[49]

$$\tau_{\mathrm{ICE}} = 5.3 \times 10^{-6}\exp(756.4/T + 273)\ (\mathrm{sec}), \quad (42)$$

$$\epsilon'_{r0\mathrm{ICE}} = 20715/(T + 273 - 38), \quad (43)$$

and

$$\epsilon'_{r\infty\mathrm{ICE}} = 3.14.$$

The effect of dc conductivity is neglected, since at the frequencies of concern here it contributes little to $\epsilon''_{r\mathrm{ICE}}$.

The air volume fraction is calculated using

$$V_{\mathrm{air}} = 1 - \frac{\rho}{0.926\ \mathrm{g/cm^3}}, \quad (44)$$

where ρ is the measured density of the sea ice and 0.926 g/cm³ is the average density of nonporous sea ice.

D. Comparison with experimental data for first-year sea ice

Figures 5–16 compare the value of ϵ'_r and ϵ''_r, calculated using Eqs. (23)–(44), and some representative experimental data.[14] Each set of curves has been evaluated at the temperature, salinity, and density of the experimental data.

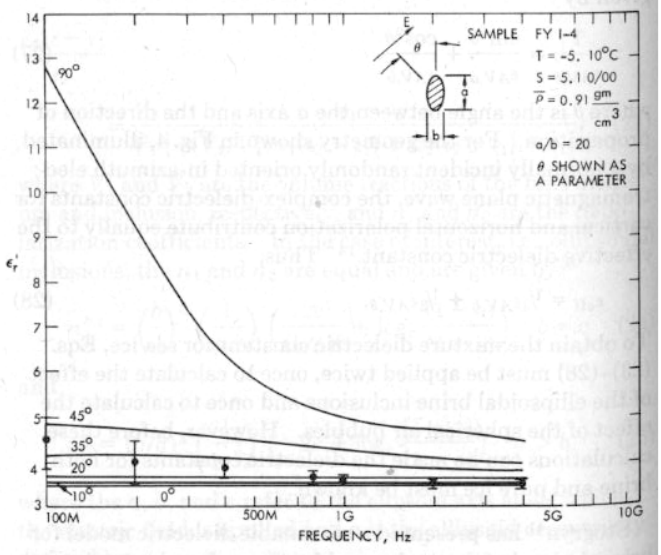

FIG. 5. Comparison of theoretical model (solid line) with experimental data for ϵ'_r, using AIDJEX sample FYI-4 (S = 5.1‰, T = −5.10 °C, and $\bar{\rho}$ = 0.91 g/cm³); angle of ellipsoids with respect to the vertical is shown as a parameter; a/b = 20.

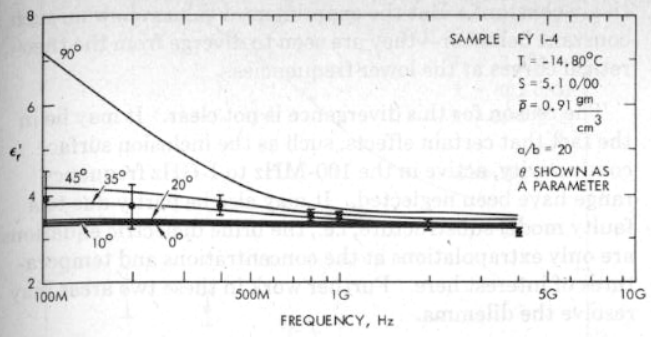

FIG. 6. Comparison of theoretical model (solid line) with experimental data for ϵ_r' using AIDJEX sample FYI-4 ($S = 5.1‰$, $T = -14.80$ °C, and $\bar{\rho} = 0.91$ g/cm^3); angle of ellipsoids with respect to the vertical is shown as a parameter; $a/b = 20$.

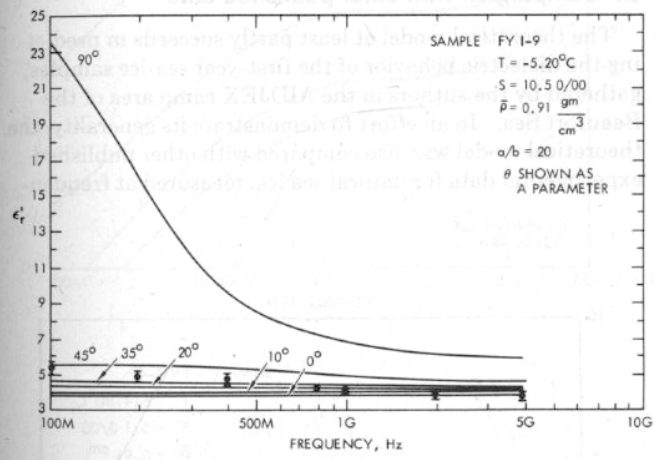

FIG. 7. Comparison of theoretical model (solid line) with experimental data for ϵ_r' using AIDJEX sample FYI-9 ($S = 10.5‰$, $T = -5.20$ °C, and $\bar{\rho} = 0.91$ g/cm^3); angle of ellipsoids with respect to the vertical is shown as a parameter; $a/b = 20$.

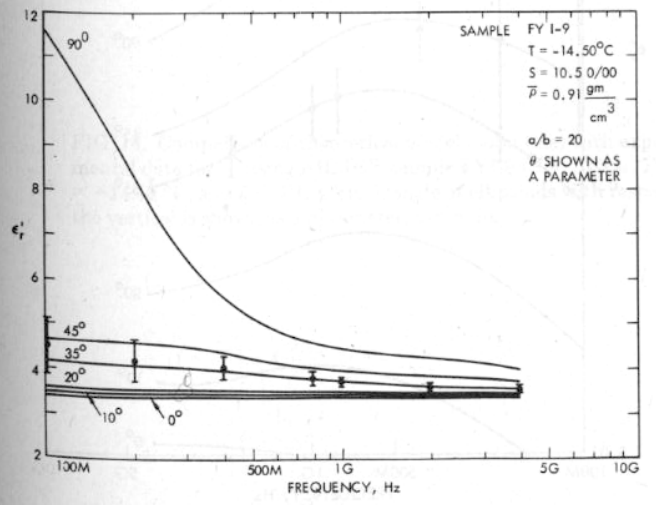

FIG. 8. Comparison of theoretical model (solid line) with experimental data for ϵ_r', using AIDJEX sample FYI-9 ($S = 10.5‰$, $T = -14.50$ °C, and $\bar{\rho} = 0.91$ g/cm^3); angle of ellipsoids with respect to the vertical is shown as a parameter; $a/b = 20$.

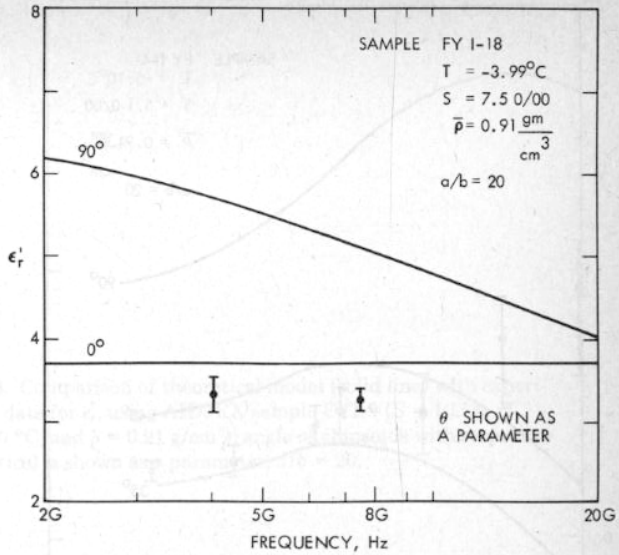

FIG. 9. Comparison of theoretical model (solid line) with experimental data for ϵ_r', using AIDJEX sample FYI-18 ($S = 7.5‰$, $T = -3.99$ °C, and $\bar{\rho} = 0.91$ g/cm^3).

The ellipsoid axial ratio was assumed to be 20 in the theoretical calculations, and in general the model predictions are determined for six different ellipsoid orientation angles; 0°, 10°, 20°, 35°, 45°, and 90°.

It should be apparent that certain trends exist in the comparison. In most cases all the experimental points for both ϵ_r' and ϵ_r'' lie between the $\theta = 35°$ and the $\theta = 45°$ curves. (a notable exception, to be discussed later, exists for the ϵ_r'' data at frequencies less than 400 MHz.) Although there are complicating influences, such as density variations in the samples, the general trend tends to suggest that in the theoretical model the fictitious ellipsoids should all lie at angles between 35° and 45° to the vertical. The gently decreasing curves obtained for ϵ_r' versus frequency are easily understood

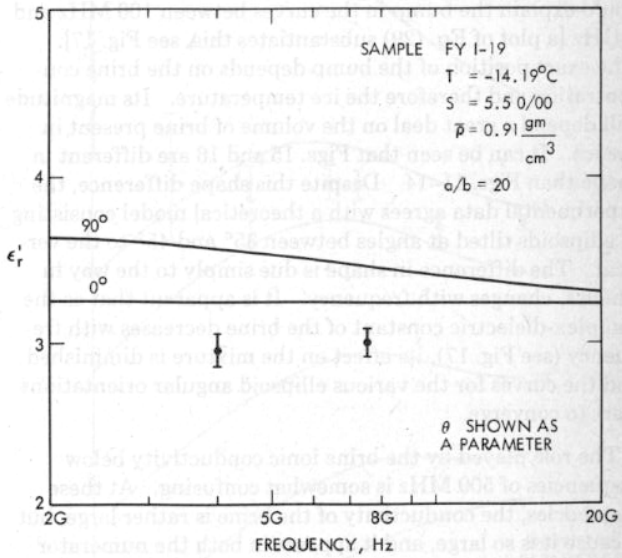

FIG. 10. Comparison of theoretical model (solid line) with experimental data for ϵ_r', using AIDJEX sample FYI-19 ($S = 5.5‰$, $T = -14.19$ °C, and $\bar{\rho} = 0.91$ g/cm^3).

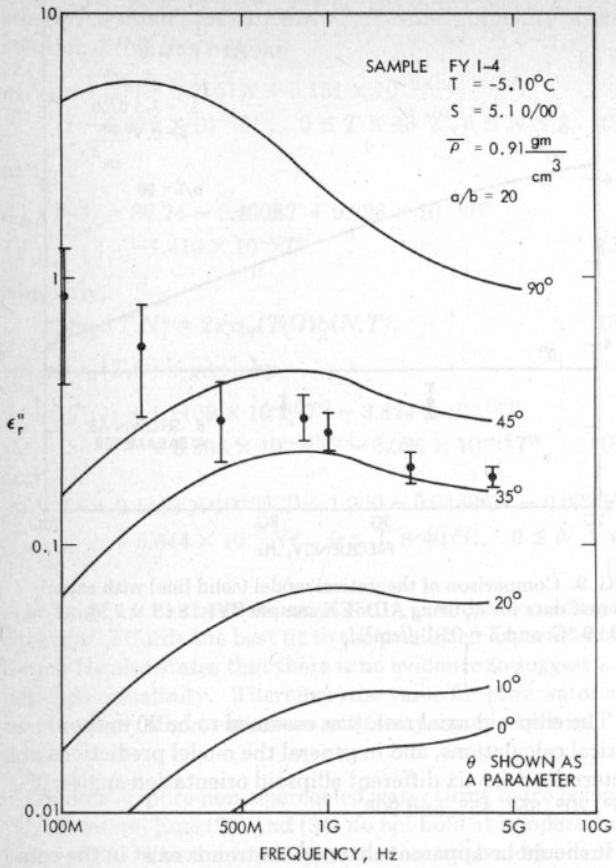

FIG. 11. Comparison of theoretical model (solid line) with experimental data for ϵ_r'', using AIDJEX sample FYI-4 ($S = 5.1‰$, $T = -5.10$ °C, and $\overline{\rho} = 0.91$ g/cm³); angle of ellipsoids with respect to the vertical is shown as a parameter; $a/b = 20$.

in view of the gradual decrease in the value of $\epsilon_{r\text{br}}'$ with frequency. The more complicated ϵ_r'' curves suggest that there is a competition for dominance between the brine conductivity and relaxation mechanisms. The relaxation of the brine could explain the bump in the curves between 100 MHz and 5 GHz [a plot of Eq. (29) substantiates this, see Fig. 17]. The exact position of the bump depends on the brine concentration and therefore the ice temperature. Its magnitude will depend a great deal on the volume of brine present in the ice. It can be seen that Figs. 15 and 16 are different in shape than Figs. 11–14. Despite this shape difference, the experimental data agrees with a theoretical model consisting of ellipsoids tilted at angles between 35° and 45° to the vertical. The difference in shape is due simply to the way in which ϵ_r'' changes with frequency. It is apparent that as the complex-dielectric constant of the brine decreases with frequency (see Fig. 17), its effect on the mixture is diminished and the curves for the various ellipsoid angular orientations start to converge.

The role played by the brine ionic conductivity below frequencies of 500 MHz is somewhat confusing. At these frequencies, the conductivity of the brine is rather large, but because it is so large, and it appears in both the numerator and denominator of the mixture equations, its effect is partially cancelled. A comparison of the theoretical ϵ_r'' curves for various temperatures and salinities shows that ϵ_r'' is relatively constant. But the experimental values show no such constant behavior—they are seen to diverge from the theoretical curves at the lower frequencies.

The reason for this divergence is not clear. It may lie in the fact that certain effects, such as the inclusion surface conductivity, active in the 100-MHz to 1-GHz frequency range have been neglected. It may also be partly due to a faulty model substructure, i.e., the brine dielectric equations are only extrapolations at the concentrations and temperatures of interest here. Further work in these two areas may resolve the dilemma.

Despite these drawbacks the theoretical model succeeds in predicting the values of ϵ_r' and ϵ_r'' for first-year ice, reasonably accurately, over the frequency range 400 MHz to 7.5 GHz, and over the temperature and salinity ranges −4 to −15 °C and 5–10.5‰, respectively.

E. Comparison with other published data

The theoretical model at least partly succeeds in predicting the dielectric behavior of the first-year sea-ice samples, gathered by the authors in the AIDJEX camp area of the Beaufort Sea. In an effort to demonstrate its generality, the theoretical model was also compared with other published experimental data for natural sea ice, measured at frequen-

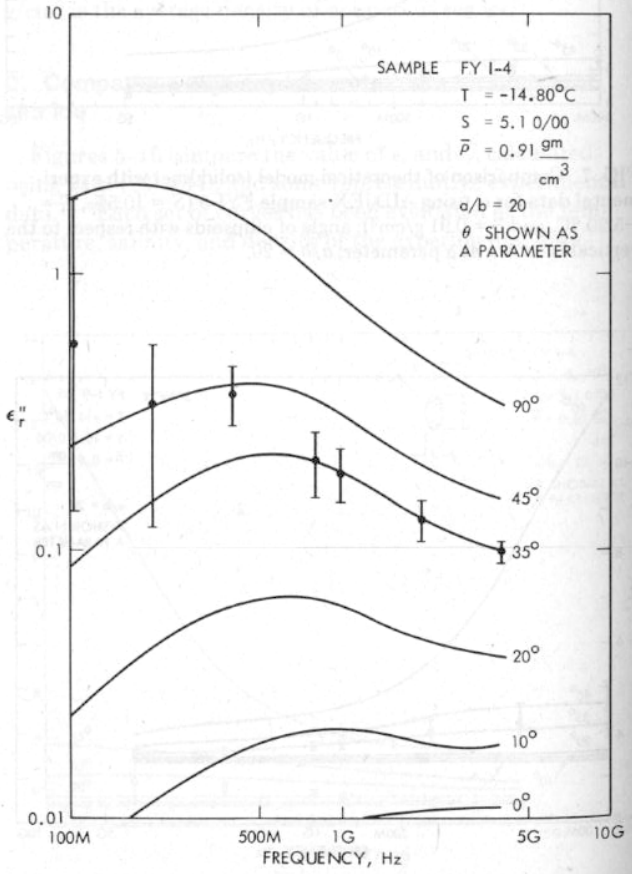

FIG. 12. Comparison of theoretical model (solid line) with experimental data for ϵ_r'', using AIDJEX sample FYI-4 ($S = 5.1‰$, $T = -14.80$ °C, and $\overline{\rho} = 0.91$ g/cm³); angle of ellipsoids with respect to the vertical is shown as a parameter; $a/b = 20$.

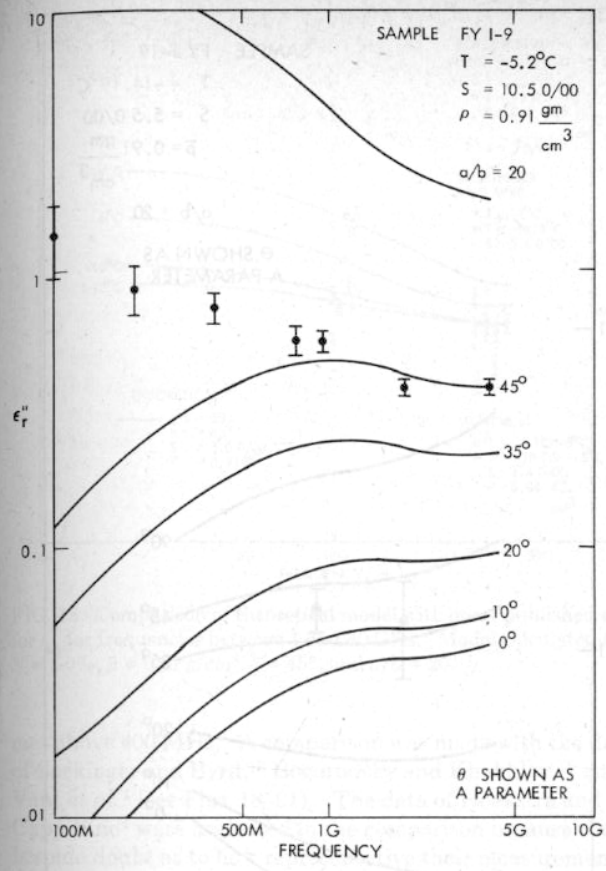

FIG. 13. Comparison of theoretical model (solid line) with experimental data for ϵ_r'', using AIDJEX sample FYI-9 ($S = 10.5‰$, $T = -5.20$ °C, and $\bar{\rho} = 0.91$ g/cm^3); angle of ellipsoids with respect to the vertical is shown as a parameter; $a/b = 20$.

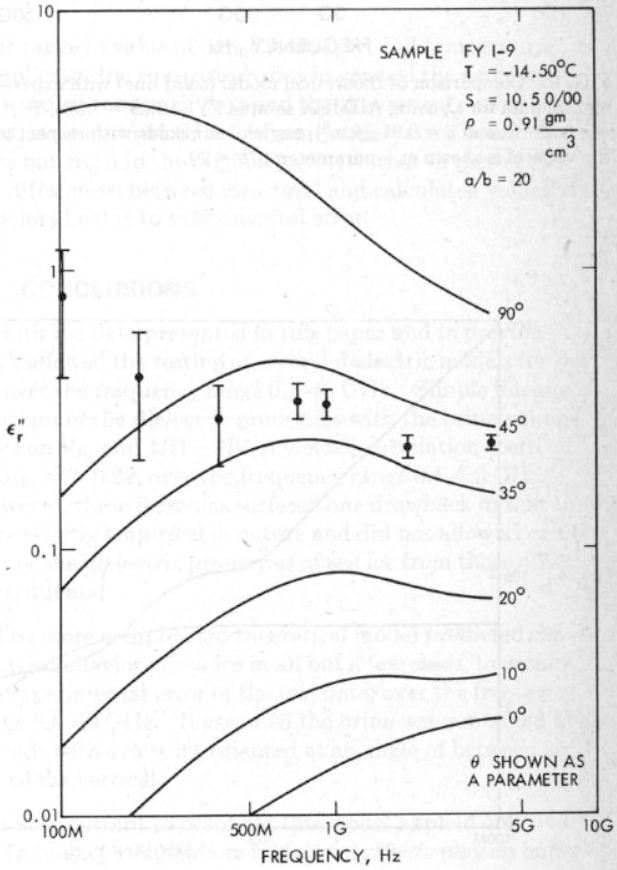

FIG. 14. Comparison of theoretical model (solid line) with experimental data for ϵ_r'', using AIDJEX sample FYI-9 ($S = 10.5‰$, $T = -14.50$ °C, and $\bar{\rho} = 0.91$ g/cm^3); angle of ellipsoids with respect to the vertical is shown as a parameter; $a/b = 20$.

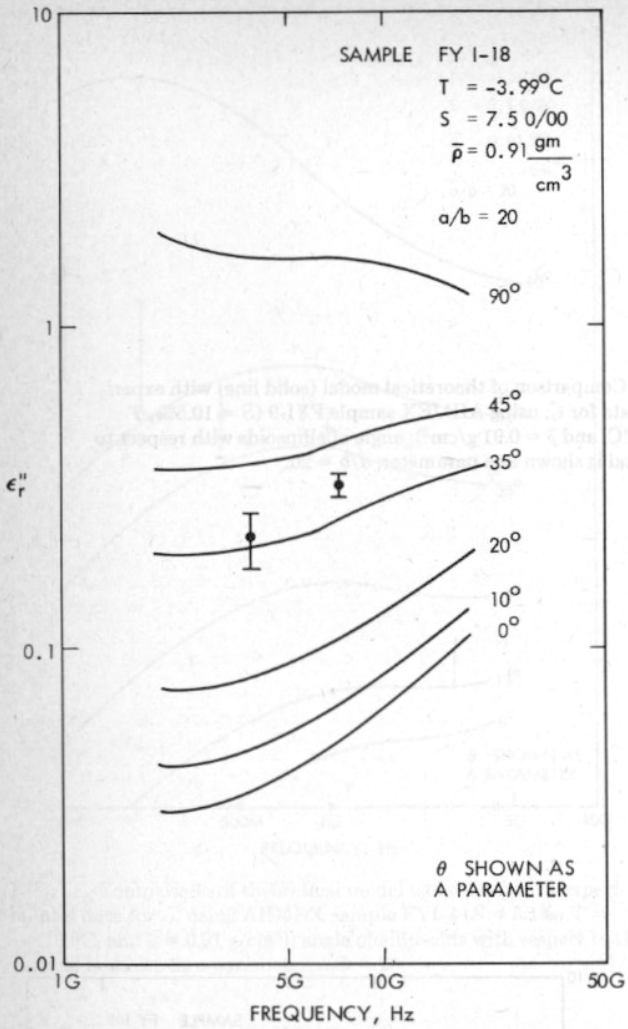

FIG. 15. Comparison of theoretical model (solid line) with experimental data for ϵ_r'', using AIDJEX sample FYI-18 ($S = 7.5‰$, $T = -3.99$ °C, and $\bar{\rho} = 0.91$ g/cm³); angle of ellipsoids with respect to the vertical is shown as a parameter; $a/b = 20$.

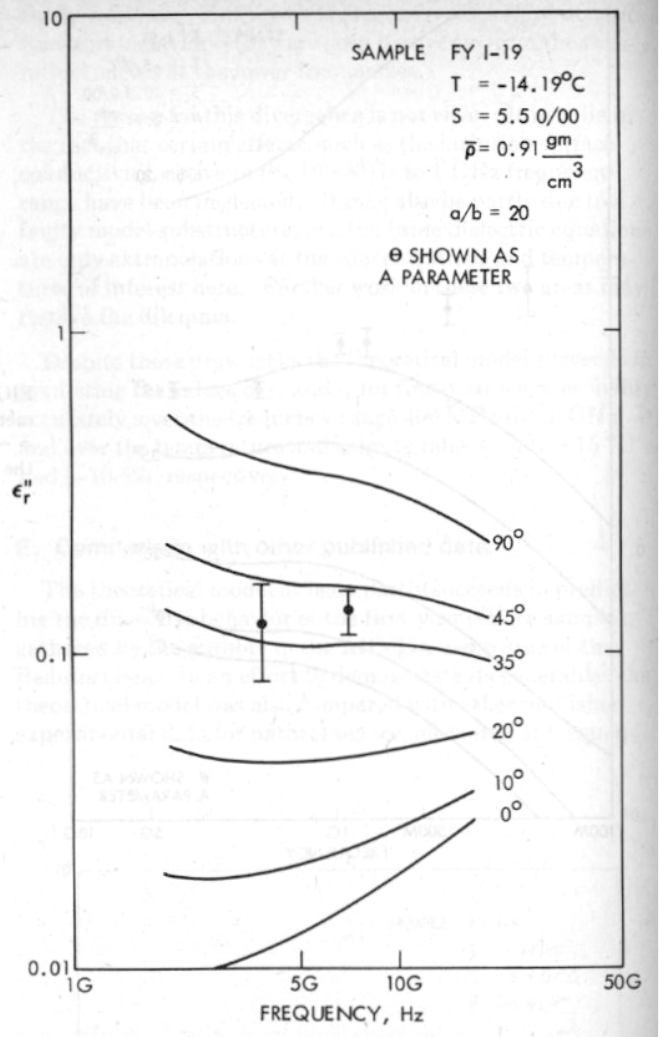

FIG. 16. Comparison of theoretical model (solid line) with experimental data for ϵ_r'', using AIDJEX sample FYI-19 ($S = 5.5‰$, $T = -14.19$ °C, and $\bar{\rho} = 0.91$ g/cm³); angle of ellipsoids with respect to the vertical is shown as a parameter; $a/b = 20$.

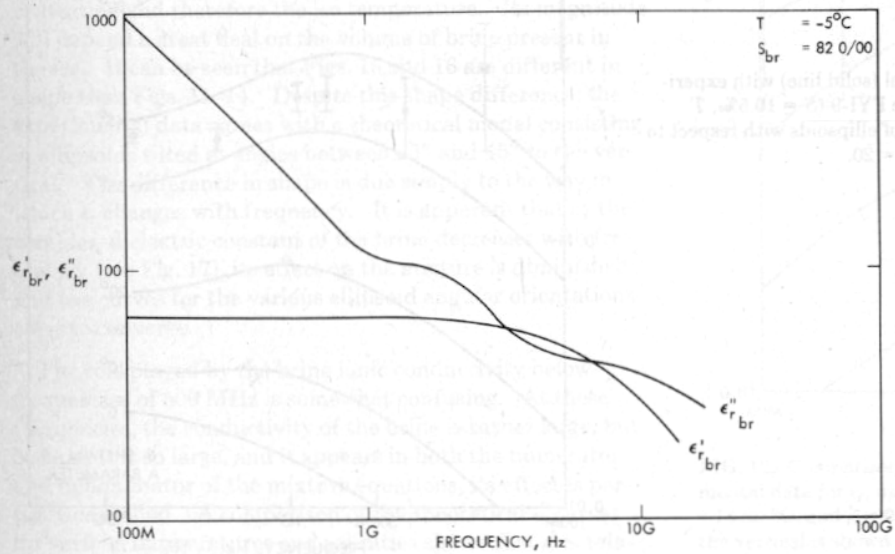

FIG. 17. $\epsilon_{r_{br}}'$, $\epsilon_{r_{br}}''$ versus frequency for $T = -5$ °C and $S = 82‰$.

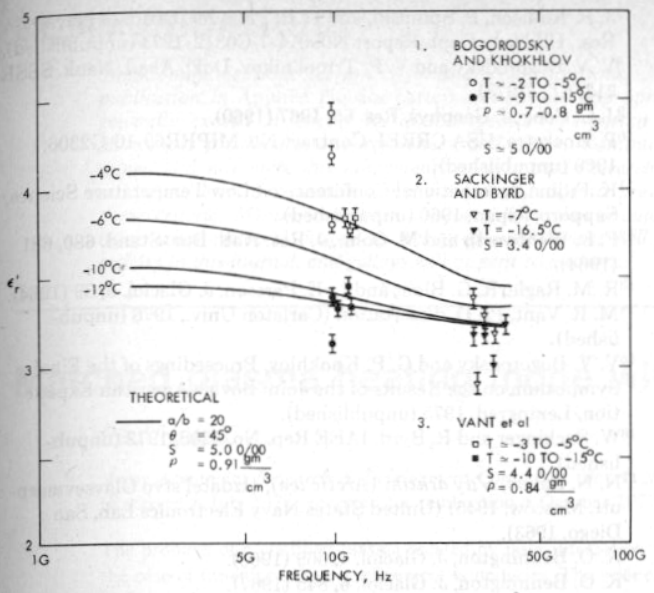

FIG. 18. Comparison of theoretical model with other published data for ϵ_r', for frequencies between 1 and 40 GHz. Model calculated for $S = 5.0‰$, $\bar{\rho} = 0.91$ g/cm^3, $\theta = 45°$, and $a/b = 20$.

cies above 400 MHz. A comparison was made with the data of Sackinger and Byrd,[16] Bogorodsky and Khokhlov,[15] and Vant *et al.*[1] (see Figs. 18–21). The data of Hoekstra and Cappillino[4] were neglected in the comparison because there is some doubt as to how representative their measurements, on quickly frozen sea water contained in a coaxial line, are of natural sea ice. For purposes of comparison, the theoretical curves were generated over the frequency range of interest, using an axial ratio of 20 and a value for θ of 45°. The density was assumed to be 0.91 g/cm^3. Figures 18–21 were prepared for two salinities, 5 and 8‰ and five temperatures, −4, −6, −10, −12, and −14 °C. The range of values inherent in the plotted data from each source is given in each figure.

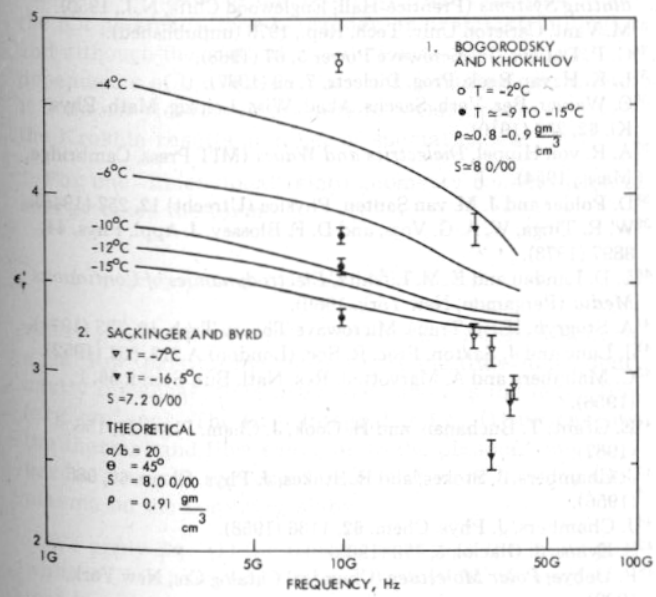

FIG. 19. Comparison of theoretical model with other published data for ϵ_r', for frequencies between 1 and 40 GHz. Model calculated for $S = 8.0‰$, $\bar{\rho} = 0.91$ g/cm^3, $\theta = 45°$, and $a/b = 20$.

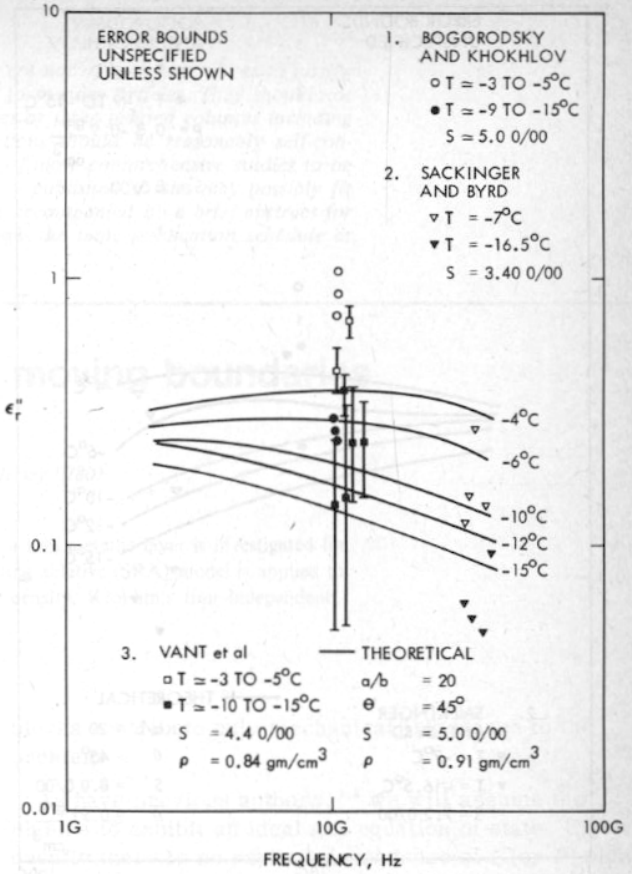

FIG. 20. Comparison of theoretical model with other published data for ϵ_r'', for frequencies between 1 and 40 GHz. Model calculated for $S = 5.0‰$, $\bar{\rho} = 0.91$ g/cm^3, $\theta = 45°$, and $a/b = 20$.

This range in value of density, salinity, and temperature complicates the comparison, but in general the agreement between all sources of data and the theoretical curves is very good, even up to 40 GHz. In many cases, error bounds for ϵ_r'' were not given in the original paper, so that in these cases the differences between measured and calculated values of ϵ_r'' may just be due to experimental error.

VII. CONCLUSIONS

Both the data presented in this paper and in previous work allowed the testing of several dielectric models for sea ice over the frequency range 0.1–40 GHz. Simple linear correlations of the dielectric properties with the brine-volume fraction V_{br} and $1/(1 - 3V_{br})$ yielded correlation coefficients, $r^2 > 0.69$, over the frequency range 0.1–7.5 GHz. However, these formulas suffered one drawback in that they were strictly empirical in nature and did not allow a prediction of the dielectric properties of sea ice from those of its constituents.

The more complicated theoretical model predicted the dielectric behavior of sea ice in all but a few cases, to within the experimental error of the test data, over the frequency range 0.4–40 GHz. It assumed the brine was contained in ellipsoids with $a/b = 20$, oriented at an angle of between 35° to 45° to the vertical.

It is important to note that this model applied only over the frequency range where interfacial effects play an impor-

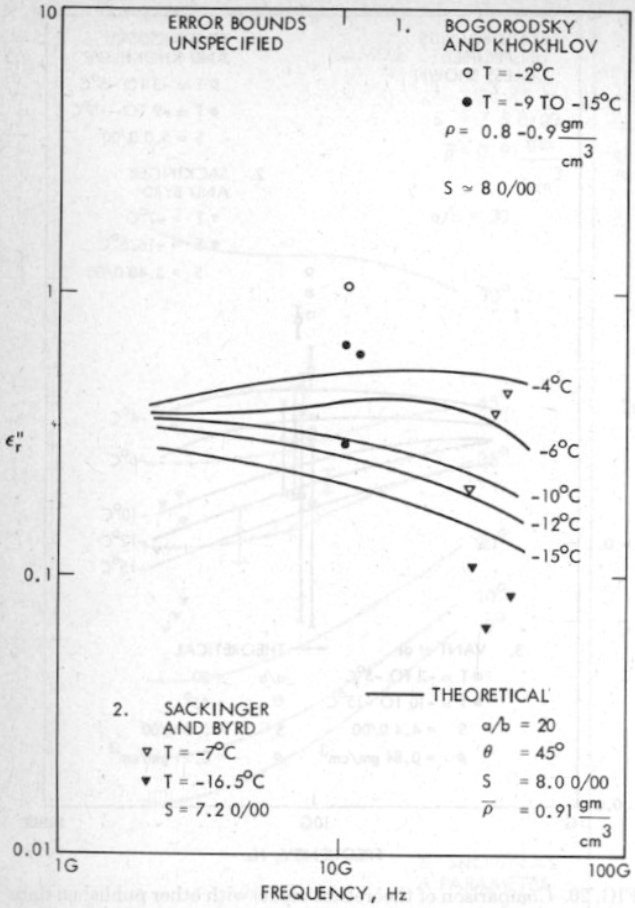

FIG. 21. Comparison of theoretical model with other published data for ϵ_r'', for frequencies between 1 and 40 GHz. Model calculated for $S = 8.0‰$, $\bar{\rho} = 0.91$ g/cm^3, $\theta = 45°$, and $a/b = 20$.

tant role in determining the mixture's dielectric properties and where scattering losses are minimal. Incorporation in the model of better dielectric information for highly concentrated brine solutions, at temperatures below 0 °C, should significantly improve its accuracy.

ACKNOWLEDGMENTS

The authors would like to acknowledge the support of the following agencies during the AIDJEX experiment. The Polar Continental Shelf Project of the Department of Energy, Mines and Resources, and the AIDJEX project office. They would also like to thank D. Y. Waung and R. B. Gray for their helpful comments and suggestions, and R. J. Weaver, M. Holtz, and A. Redmond for their technical assistance.

[1]M. R. Vant, R. B. Gray, R. O. Ramseier, and V. Makios, J. Appl. Phys. **45,** 4712 (1974).
[2]J. R. Addison, J. Appl. Phys. **40,** 3105 (1969).
[3]J. R. Addison, J. Appl. Phys. **41,** 54 (1970).
[4]P. Hoekstra and P. Cappillino, J. Geophys. Res. **76,** 4922 (1971).
[5]J. R. Addison and E. R. Pounder, USAF Rep. AFCRL-64-52, 1964 (unpublished).
[6]J. R. Addison and E. R. Pounder, International Conference on Low Temperature Science, Sapporo, Japan, 1967 (unpublished).
[7]J. R. Addison, P. Stalinski, and E. R. Pounder, Office of Naval Res., US Navy Dept. Report N00014-7-C0312, 1974 (unpublished)
[8]V. V. Bogorodsky and V. P. Tripol'nikov, Dokl. Akad. Nauk. SSS **213,** 577 (1973).
[9]J. C. Cook, J. Geophys. Res. **65,** 1967 (1960).
[10]P. Hoekstra, USA CRREL Contract No. MIPRR69-10-G2306, 1969 (unpublished).
[11]K. Fujino, International Conference on Low Temperature Scienc Sapporo, Japan, 1966 (unpublished).
[12]F. L. Wentworth and M. Cohn, J. Res. Natl. Bur. Stand. **680,** 681 (1964).
[13]R. M. Ragle, R. G. Blair, and L. E. Persson, J. Glaciol. **5,** 39 (1964
[14]M. R. Vant, Ph.D. dissertation (Carleton Univ., 1976 (unpublished).
[15]V. V. Bogorodsky and G. P. Khokhlov, Proceedings of the Final Symposium on the Results of the Joint Soviet-American Expedition, Leningrad, 1975 (unpublished).
[16]W. Sackinger and R. Byrd, IAEE Rep. No. 7203, 1972 (unpublished).
[17]N. N. Zubov, *L'dy arktiki* (*Arctic ice*), (Izdatel'stvo Glavsevmorp uti, Moscow, 1945) (United States Navy Electronics Lab, San Diego, 1963).
[18]K. O. Bennington, J. Glaciol. **4,** 669 (1963).
[19]K. O. Bennington, J. Glaciol. **6,** 845 (1967).
[20]R. A. Lake and E. L. Lewis, J. Geophys. Res. **75,** 583 (1970).
[21]L. I. Eide and S. Martin, J. Glaciol. **14,** 137 (1975).
[22]G. A. Poe, A. Stogryn, A. T. Edgerton, and R. O. Ramseier, Aeroje Electrosystems Co. Final Rep. No. 1804 FR-1, Contract No. 2-35424, 1974 (unpublished).
[23]E. R. Pounder, *The Physics of Ice* (Pergamon, New York, 1965).
[24]W. R. Weeks and G. F. N. Cox, USA CRREL Special Rep. 206, 1974 (unpublished).
[25]A. Assur, USA Cold Regions Research and Engineering Laboratory, Res. Rep. 44, 1960 (unpublished).
[26]G. Frankenstein and R. Garner, J. Glaciol. **6,** 943 (1967).
[27]G. Poe, A. Stogryn, and A. T. Edgerton, Aerojet Electrosystems Co. Final Technical Rep. 1749R-2, Contract No. 2-3530, 1972 (unpublished).
[28]M. Kerker, *The Scattering of Light and Other Electromagnetic Radiation* (Academic, New York, 1969).
[29]R. W. P. King, *Transmission-Line Theory* (McGraw-Hill, New York, 1955).
[30]J. R. Addison, Rev. Sci. Instrum. **46,** 101 (1975).
[31]Hewlett-Packard 1976 Catalog, Hewlett-Packard Ltd. (Palo Alta, Calif.).
[32]E. C. Jordan and K. G. Balmain, *Electromagnetic Waves and Radiating Systems* (Prentice-Hall, Englewood Cliffs, N.J., 1950).
[33]M. Vant, Carleton Univ. Tech. Rep., 1973 (unpublished).
[34]G. P. DeLoor, J. Microwave Power **3,** 67 (1968).
[35]L. K. H. van Beek, Prog. Dielectr. **7,** 69 (1967).
[36]O. Weiner, Ber. Verh. Saechs. Akad. Wiss. Leipzig, Math. Phys. Kl. **62,** 256 (1910).
[37]A. R. von Hippel, *Dielectrics and Waves* (MIT Press, Cambridge, Mass., 1954).
[38]D. Polder and J. M. van Santen, Physica (Utrecht) **12,** 257 (1946).
[39]W. R. Tinga, W. A. G. Voss, and D. F. Blossey, J. Appl. Phys. **44,** 3897 (1973).
[40]L. D. Landau and E. M. Lifshitz, *Electrodynamics of Continuous Media* (Pergamon, New York, 1960).
[41]A. Stogryn, IEEE Trans. Microwave Theory Tech. **19,** 733 (1971).
[42]J. Lane and J. Saxton, Proc. R. Soc. (London) A **213,** 531 (1952).
[43]C. Malmberg and A. Maryott, J. Res. Natl. Bur. Stand. **56,** 1 (1956).
[44]E. Grant, T. Buchanan, and H. Cook, J. Chem. Phys. **26,** 156 (1957).
[45]J. Chambers, J. Stokes, and R. Stokes, J. Phys. Chem. **60,** 985 (1956).
[46]J. Chambers, J. Phys. Chem. **62,** 1136 (1958).
[47]S. Evans, J. Glaciol. **5,** 773 (1965).
[48]P. Debye, *Polar Molecules* (Chemical Catalog Co., New York, 1929).
[49]Y. Ozawa and D. Kuroiwa, Research Institute of Applied Electricity, edited by Y. Asami, Sapporo, Japan, 1958, pp. 31–71 (unpublished).